Seismicity and Seismic Hazard Assessment for the Magadan Region on a Scale Close to Detailed Seismic Zoning

A. I. Lutikov[a, b,]*, N. V. Andreeva[b], I. P. Gabsatarova[a], G. Yu. Dontsova[a], and L. I. Karpenko[c]

[a]*United Geophysical Survey of the Russian Academy of Sciences, Obninsk, Moscow, 249035 Russia*
[b]*Schmidt Institute of Physics of the Earth, Russian Academy of Sciences, Moscow, 123242 Russia*
[c]*Magadan Branch of the Geophysical Survey, Russian Academy of Sciences, Magadan, 685024 Russia*
*e-mail: ail@ifz.ru

Abstract—This paper presents the results of a seismic hazard assessment for the Magadan region (quadrangle $58.5°-66.0°$ N, $143.3°-157.7°$ E) in terms of macroseismic scale units. The extent of the research corresponds to the regional one (in the terminology framework accepted in Russia, this corresponds to the scale of the detailed seismic zoning (DSZ)). The seismic activity matrix ($A_{3.3}$) is obtained and the following main seismicity parameters are estimated: the slope of the recurrence graph, the average thickness of the seismoactive layer, and depth of this layer (h); on the basis of the obtained results, when constructing seismic intensity maps, the focal depth we used was $h = 10$ km. Proceeding from the analysis of comprehensive seismological, tectonic, and geological data, 13 zones of possible earthquake sources (PES zones) with $M_{max} = 6.5, 7.0$ and 7.5 were distinguished in the Magadan region . Beyond the identified zones, the background seismicity was assumed to be $M_{max} = 5.0$. The study resulted in obtaining probabilistic seismic hazard maps of the Magadan region in terms of macroseismic scale intensity units, calculated for average recurrence periods of 500, 1000, and 5000 years.

Keywords: seismic hazard, macroseismic intensity, recurrence graph, seismic activity, PES zones, seismic shaking

INTRODUCTION

The northeastern Russian Federation, a considerable part of which is occupied by the Magadan region, is an area of high seismic hazard. According to the GSZ-2015 (OSR-2015) General Seismic Zoning maps, this region is characterized by zones with potential seismic shaking intensities of VII, VIII, and IX, according to the current macroseismic scale (MSK-64). This means that studies which aim to provide a seismic hazard assessment for the Magadan region on a scale close to that of detailed seismic zoning (DSZ), are extremely topical.

According to (*Seismicheskaya sotryasaemost'*..., 1979), the Magadan region can be subdivided into three parts in terms of macroseismic manifestations: south, center, and northeast. The southern and northeastern parts of the Magadan region are seismic, while the central one is nearly aseismic. Due to its relatively denser population and quite intensive economic activity, the southern part is the most important for seismic hazard assessment. The southern part of the Magadan region is confined by the coordinates $58.0°-65.0°$ N and $144.0°-162.0°$ E (*Seismicheskaya sotryasaemost'*..., 1979). Six earthquakes with $M_S \geq 6.0$ (maximum magnitude was $M_S = 7.1$) have occurred here over the past 170 years, indicating the moderately high seismic activity of this area.

Several works on the seismicity and seismic hazard of the Magadan region have been published in recent years (Sharafutdinov, 2009; Bespalov, 2015; Mishin and Khasanov, 2016). These studies dealt with mapping seismic activity and its spatiotemporal changes in the period from 1968 to 2013. Note that the boundaries of the area studied in these publications approximately fitted the aforementioned limits of the southern part of the Magadan region.

The present work is dedicated to a seismic hazard assessment of the southern part of the Magadan region limited by coordinates $58.5°-66.0°$ N and $143.3°-157.7°$ E, approximately fitting the areas studied in previous works. The total area, for which seismic hazard is to be assessed, is therefore about 618 000 km².

We present the results of the seismic regime study, including the determination of recurrence law parameters, matrix of seismic activity, and distribution of earthquake hypocenters in depth. Based on the analysis of geological-geophysical and seismological data, we propose a scheme of zones of possible earthquake sources (PES zones), and the M_{max} matrix is constructed by the digitization of this scheme. The final result of the present work is a seismic hazard assessment in terms of macroseismic intensity points. The probabilities of these being exceeded are 1%, 5%, and 10% for the 50-year period. Macroseismic intensity is determined by calculating seismic shaking using Yu.V.
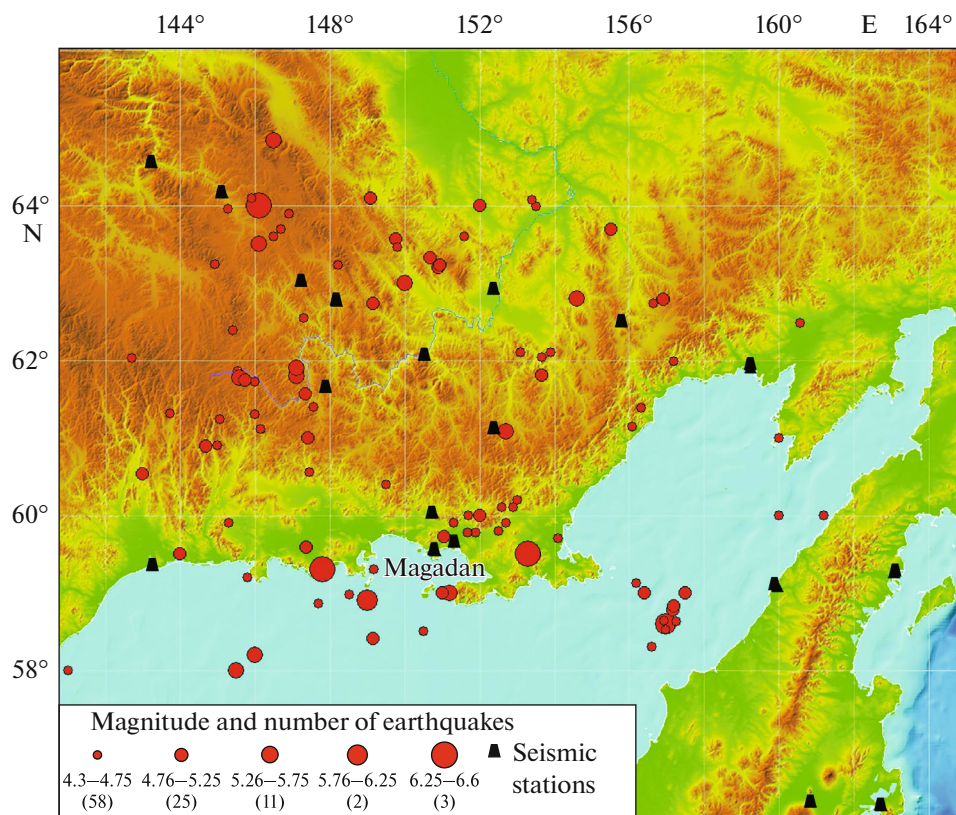
Fig. 1. Map of epicenters of strong and moderate earthquakes ($M_S \geq 4.3$) for the entire time period of the UAC (99 earthquakes in total).

Riznichenko's method (*Seismicheskaya sotryasae-most'...*, 1979). It should be noted that Riznichenko's method is, in our opinion, the optimal in the present case for seismic hazard assessment in terms of macro-seismic shaking intensity.

The methodical basis of the works carried out is the new *SP* (Rules and Regulations) *408.1325800.2018: Detailed Seismic Zoning and Seismic Microzoning for the Territory Planning*.

INITIAL SEISMOLOGICAL DATA

The data for the present study were taken from the following sources:

(1) catalog of the Magadan Branch of the Geophysical Survey, Russian Academy of Sciences (MB GS RAS), with the removed aftershocks;

(2) *Unified Catalog of Earthquakes in Northern Eurasia since Ancient Times through 2013* (hereinafter, UCENE), beginning from magnitudes $M = 3.5$ (Ulomov and Medvedeva, 2013);

(3) CMT catalog (Global CMT..., 2019).

Based on these sources, the aggregated earthquake catalog was compiled for the purpose of the present study; it included all events that occurred within the latitude and longitude ranges of $\varphi = 58.0°{-}66.0°$ N and $\lambda = 142.0°{-}160.0°$ E, respectively, in the period

from 1735 to 2015. After the exclusion of all earthquakes which were a priori not representative for the entire area under study ($M_S \leq 1.7$), the aggregated catalog included 3052 events with $1.8 \leq M_S \leq 7.1$.

The accuracy of the determination of earthquake parameters changed as the seismic network developed in the region. The parameters of historical earthquakes, as estimated by B.M. Koz'min and T.A. Andreev [1977], presented in (*Novyi katalog...*, 1977) and later in the UCENE, according to expert assessment, had errors in the determination of epicentral coordinates $\delta\varphi$ and $\delta\lambda = \pm0.5°$ or even $\pm1.0°$, while errors in determination of depths were $\pm h$ km. Later, with the development of regional seismic networks in the 1960s, these errors were reduced: $\delta\varphi$ and $\delta\lambda$ became $\pm0.2°$ or, rarely, $\pm0.1°$, the determination of depth was $\pm0.5h$ and $\pm0.2h$. For the present-day network (Fig. 1), using the processing techniques at MB GS RAS and based on knowledge of the velocity characteristics of the medium (Mackey et al., 1998), the completeness of earthquakes with $K_{(Magadan)} \geq 7$ is provided in the territory of Magadan region; errors in determining coordinates $\delta\varphi$ and $\delta\lambda$ are no more than $\pm0.1°$, while errors in determining depth are no more than $\pm0.5h$ (Aleshina et al., 2018).

Energy class $K_{(Magadan)}$ was used in the MB GS RAS. In the aggregated catalog, all data were unified on mag-
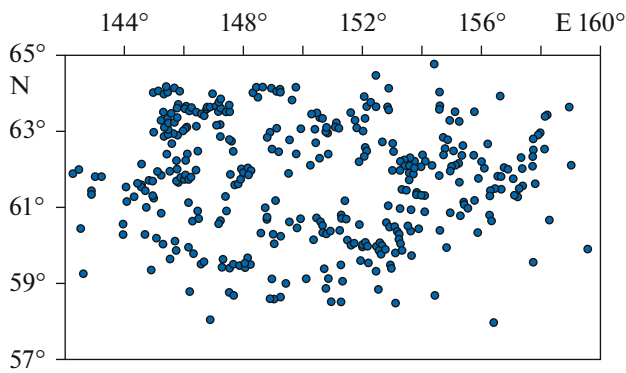
Fig. 2. Distribution of epicenters of earthquakes with $M_S = 2.0$ in 2011−2015 within the study area.

nitude M_S. The dependence between magnitude M_S (Ulomov and Medvedeva, 2013) and energy class $K_{(Magadan)}$ was calculated by the following correlation formula obtained for 53 pairs of events:

$$M_S = 0.5481\,K_{(Magadan)} - 2.1271; \quad R_c = 0.958. \quad (1)$$

The magnitude-unified aggregated catalog for the period from 1735 to 2015 (hereinafter, UAC), compiled with the use of the sources mentioned above, was used for the seismic hazard assessment of the Magadan region.

ANALYSIS OF THE SEISMIC REGIME

The territory under seismological study approximately covers the southern zone of the Magadan region. To analyze the seismic regime, we used the UAC whose compilation principles were described above. To recall, it includes 3052 events with $1.8 <$ $M_S < 7.1$ and covers the time period from 1735 to 2015. The map in Fig. 1 shows the epicenters of strong and moderate earthquakes ($M_S \geq 4.3$) for the entire period of time covered by the UAC (99 events in total).

Table 1 shows how earthquakes from the catalog are distributed in terms of time and magnitude. The periods of representative observations for different magnitudes are marked in bold. The lowest representative magnitude for the entire territory under consideration is bound to $M_S = 2.0$ (in the period from 2011 to 2015). Its representativeness in time is supported by Table 1, whereas Fig. 2 demonstrates the spatial homogeneity of the UAC in 2011−2015 on $M_S = 2.0$ over the entire area under study.

An analysis of Table 1 shows that the available seismological database is insufficient for including earthquakes with larger magnitudes ($M_S > 6.0$) in analysis when constructing the recurrence graph. In this respect, to avoid omitting events with larger magnitudes (with the respective distortion of the recurrence graph), earthquakes with $M_S > 6.0$ were excluded when constructing the recurrence graph.

After specifying the periods of representative recording of different magnitudes, the Aggregated Representative Catalog of Regional Earthquakes (ARCRE) was compiled in accordance with Table 1; it includes 2016 events in the magnitude interval of $2.0 < M_S < 6.0$ and bracketing the period from 1910 to 2015, which was used when constructing the recurrence graph. The map showing the epicenters of weak earthquakes ($M_S < 4.2$) for the same period is presented in Fig. 3.

The dependence of the number of earthquakes on earthquake magnitude $N(M)$ is called the Gutenberg−Richter recurrence law and represents one of the fundamental laws of seismology. In Table 2, events from

Table 1. Distribution of the number of events in the catalog by years and magnitude (N_{repr} is the number of representative events)

| Years/M_S	2	2.5	3	3.5	4	4.5	5	5.5	6	6.5	7	N
1701−1800	0	0	0	0	2	1	0	0	0	0	0	3
1801−1850	0	0	0	0	1	0	0	0	0	0	0	1
1851−1900	0	0	0	1	3	0	0	0	0	1	0	5
1901−1950	0	0	0	0	2	1	**7**	**3**	**3**	0	0	16
1951−1961	0	0	0	0	1	1	**1**	**0**	**0**	0	0	3
1962−1970	0	0	2	29	19	**13**	**3**	**2**	**0**	0	0	68
1971−1980	0	0	0	**59**	**23**	**10**	**2**	**3**	**0**	0	1	97
1981−1990	85	214	**110**	**41**	**20**	**5**	**3**	**0**	**0**	0	0	478
1991−1995	33	88	**80**	**19**	**10**	**5**	**0**	**0**	**0**	0	0	235
1996−2000	32	83	**113**	**65**	**24**	**6**	**1**	**0**	**1**	0	0	325
2001−2005	140	**180**	**98**	**46**	**10**	**2**	**1**	**0**	**0**	0	0	477
2006−2010	296	**189**	**74**	**35**	**7**	**3**	**1**	**0**	**0**	0	0	605
2011−2015	**435**	**198**	**73**	**15**	**11**	**2**	**3**	**1**	**0**	0	0	738
N	1021	952	550	310	133	49	22	9	4	1	1	3052
N_{repr}	435	567	548	280	105	46	22	9	4	1	1	2018
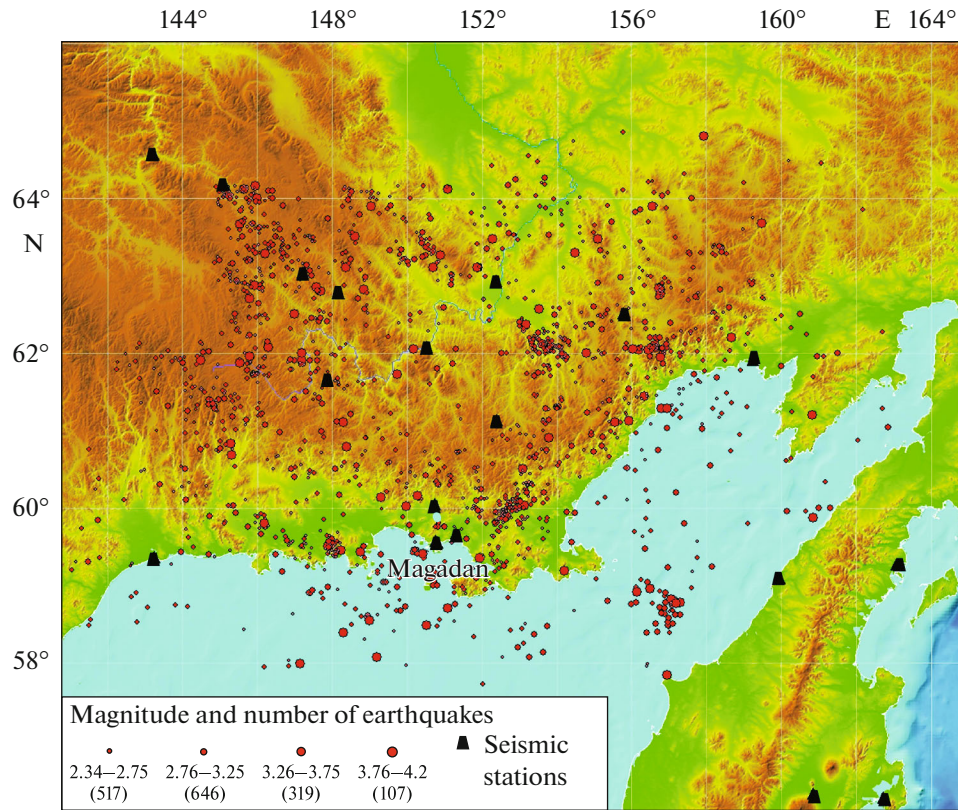
Fig. 3. Map of epicenters of weak earthquakes ($1.8 \leq M_S < 4.2$) for the period of 1910−2015 (1589 events in total).

the ARCRE are grouped on the number of events in the respective magnitude ranges, taking the period of their representative observation into account.

In Table 2, T_{repr} is the period of representative observations, in years; N, the total number of events in the respective magnitude range; and N/T_{repr}, the average number of events per year in the respective magnitude range.

Based on the data from Table 2, the non-normalized recurrence graph was constructed using the linear orthogonal regression method; it gives us some idea about the mean recurrence interval of earthquakes of the respective magnitudes over the entire area under study (Fig. 4).

In its analytical form, the recurrence graph is written as follows:

$$\log(N/T_{repr}) = -(0.880 \pm 0.022) M_S + 3.799 \pm 0.147; \quad R_c = 0.998. \quad (2)$$

A high value of linear correlation factor R_c indicates a quite high reliability of the obtained result. Based on studies in the 1960s−1970s (*Seismicheskaya sotryasae-most'*..., 1979), the angular factor of the recurrence graph relative to the energy class was $\gamma = 0.48$. Given relation (1), this parameter of the recurrence graph on

Table 2. Distribution of the number of events on intervals of representative observations and magnitudes

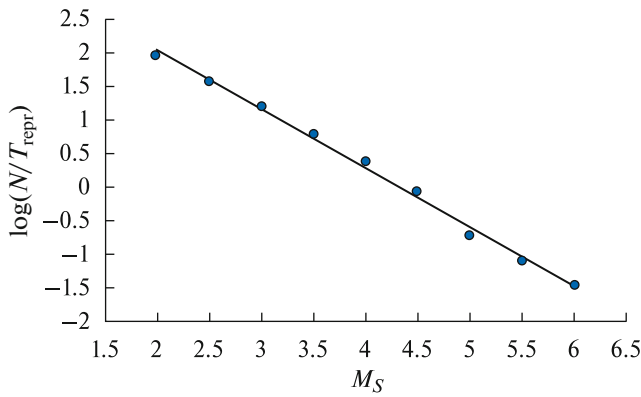| M_S	Years	T_{repr}, years	N	N/T_{repr}	$\log(N/T_{repr})$
2.0	2011−2015	5	435	87.0	1.939519
2.5	2001−2015	15	567	37.8	1.577492
3.0	1981−2015	35	548	15.65714	1.194713
3.5	1971−2015	45	280	6.222222	0.793946
4.0	1971−2015	45	105	2.333333	0.367977
4.5	1951−2015	54	46	0.851852	−0.06964
5.0	1901−2015	115	22	0.191304	−0.71828
5.5	1901−2015	115	9	0.078261	−1.10646
6.0	1901−2015	115	4	0.034783	−1.45864

Fig. 4. Recurrence graph for the magnitude interval of $2.0 < M_S < 6.0$.

magnitude M_S equals $b = \gamma/0.5481 = 0.876$, which is almost identical to the value b in formula (2). The last point indicates a high temporal stability of angular factor b.

Seismic Activity

To obtain the detailed recurrence patter of earthquakes with different magnitudes in the studied area, we constructed the matrix of seismic activity $A_{3.3}$, which is an analog of seismic activity A_{10} (*Seismicheskaya sotryasaemost'...*, 1979), also used, in combination with matrix M_{max}, to calculate seismic shaking intensity. Magnitude $M_S = 3.3$ was chosen because it corresponds to earthquakes with energy class $K = 10$, therefore, the seismic activity assessed in earlier studies remains comparable to modern results. In the seismic activity matrix $A_{3.3}$, the values of seismic activity are assigned to the centers of cells of the coordinate mesh. Calculations were made for cells with sizes of $1/6°$ on latitude and $1/3°$ on longitude. To recall, seismic activity is determined as follows

$$A_0 = \frac{\left(1 - 10^{-b}\right)}{10^{-b(M_{min} - M_0)}} \frac{T_0 S_0}{TS} N_S, \qquad (3)$$

where b is the angular factor of the recurrence graph (in the present case, $b = -0.880$); $M_{min} = 2.0$, the least representative magnitude (representativity level); $M_0 = 3.33$, the earthquake magnitude, to which the calculated activity A_0 (in the present case, $A_{3.33}$ or A_{10}) corresponds; S, the area of site of averaging, km^2; T, the period of representative observation of earthquakes, years; S_0, the unit of normalization on area, assumed in accordance with A_0 (in present case, $S_0 = 1000$ km^2); T_0, the time unit (1 year); N_S, the total number of earthquakes of various magnitudes $M \geq M_{min}$, observed for the time T within the area S.

In fact, seismic activity A_0 is the average number of earthquakes with magnitude M_0 that occurred over one year in the area of 1000 km^2. Seismic activity was

calculated using SEIACT2m software written in FORTRAN programming language.

To exemplify, Table 3 lists a fragment of the matrix of seismic activity $A_{3.3}$ calculated by formula (3), because the entire matrix is too big to be provided here.

The full matrix $A_{3.3}$ was calculated for coordinates $58.5°-66.0°$ N and $142.33°-157.67°$ E. The maximum values of seismic activity $A_{3.3}$ in the considered area reach 0.103. The matrix of seismic activity we used to calculate seismic shaking was slightly corrected, taking the scheme of PES zones into account.

Distribution of Hypocenters on Depth

The distribution of earthquake hypocenters on depth is an important element of seismic regime studies, which allows researchers to infer the depths of the seismoactive layer and its thickness in the area under study. These data are also necessary for calculating seismic shaking.

When determining hypocentral depths, MB GS RAS researchers use velocity characteristics of the medium (Mackey et al., 1998), which provide accuracy in determining hypocentral depth of $\pm 0.5h$; for hypocentral depths determined earlier, this accuracy is lower, up to $\pm h$. Thus, the distributions presented below are only approximate images of the real depth distribution of seismicity, however, no other data are currently available.

An idea about the depth distribution of seismicity within the study area can be gained from Fig. 5 which shows hypocentral depths of moderate to strong ($4.3 \leq M_S \leq 7.1$) and weak ($2.3 \leq M_S \leq 4.2$) earthquakes. These distributions are constructed based on 84 and 1544 seismic events, respectively. Note that in both cases we excluded the events with zero and standard crustal focal depths ($h = 33$ km) from consideration.

It is seen in Fig. 5a that about 87 percent of all hypocenters are clustered in the surface layer of 20 km thick; at greater depths, the number of hypocenters quickly decreases. The maximum of hypocenters is observed at depths of $5-20$ kilometers, concentrating about 74 percent of hypocenters. This depth interval can be considered the seismoactive layer for strong and moderate earthquakes.

The depth distribution of hypocenters of weak ($2.3 \leq M_S \leq 4.2$) earthquakes (Fig. 5b) shows that in this case about 78 percent of hypocenters are clustered in the uppermost 10-kilometer crustal layer. Below it, the number of hypocenters quickly decreases with depth, so that only rare seismic activity is observed at depths of more than 40 kilometers.

In our calculations of seismic shaking, hypocentral depth is assumed to be $h = 10$ kilometers, corresponding to the maximum distribution in Fig. 5.
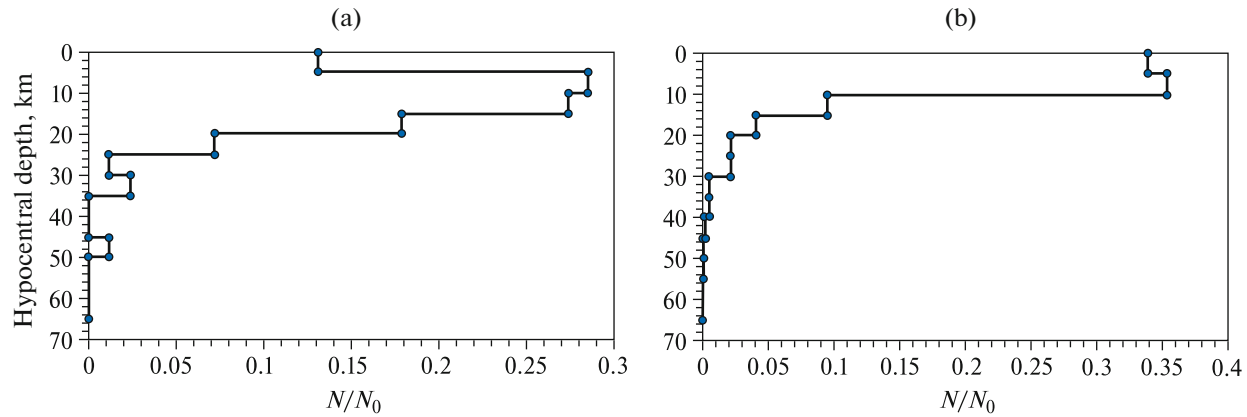
Fig. 5. Distribution of hypocenters of earthquakes on depth: (a) moderate and strong ($4.3 \leq M_S \leq 7.1$); (b) weak ($2.3 \leq M_S \leq 4.2$).

SEISMOTECTONICS AND PES ZONES

Distinguishing zones of possible earthquake sources (PES zones) for the Magadan region was done on the basis of seismological and geological data. PES zones differ in classes based on maximal magnitude M_{max} of the earthquake that can occur there. In turn, the M_{max} value is defined from the complex of geological-geophysical, geomorphic, and neotectonic data, namely, from the length and segmentation of seismoactive faults, level of seismicity, dimensions of ancient and modern seismodislocations, and results of tectonophysical studies.

The structural (spatial) peculiarities of seismic activity distribution in the Magadan region are presented in the map of seismolineaments of East Siberia, compiled by V.S. Imaev and his co-authors (2015). This map became the basis of distinguishing PES zones for the seismic hazard assessment of the region under study (Imaev et al., 2015). The small scale of this map taken as the basis, a high degree of generalization of the initial data, and a low accuracy of data binding lead to the necessity of specifying faults positions in accordance with the collected geological-geophysical data, and this is a necessary stage of a detailed seismic hazard assessment.

Seismolineaments distinguished in the map by Imaev et al. (2015) were compared to the faults imaged in the respective state geological map (*Gosudarstvennaya...*, 1992) and maps from the database in (Bachmanov et al., 2017), and their positions were specified from topography, satellite images, and large-scale overview geological maps. In addition, we took into account the tectonic positions, kinematics, and ages of the most recent displaced units, slip rates, and manifestations of recent and Holocene activity (*Gosudarstvennaya...*, 1992; Smirnov, 2000). The magnitude potential of seismolineaments was estimated from the data of earthquake catalogs (for example, UAC), containing information about the earthquakes of the instrumental period, and from the presence of paleoseismodislocations (Vazhenin, 2000; Smirnov, 2000).

We also took into account magnitudes, positions, kinematics, and earthquake focal mechanisms (Imaev et al., 2000). The magnitude of individual seismogenerating segments was estimated from their lengths in accordance with the known dependence (Wells and Coppersmith, 1994), $M_{max} = 4.38 + 1.49 \log L$, where L is the length of near-surface fault (in kilometers).

The widths of PES zones were estimated by the dependence proposed by Yu. V. Riznichenko (1976): $\log W = 0.405 M_{max} - 1.464$, where W is the width of PES zone (in kilometers).

Note that axes of PES zones were assumed to be the respective active faults and seismolineaments. We also took into consideration the scatter in locations of active faults, an in some cases several faults were united within the limits of one PES zone.

In accordance with the above, 13 PES zones were distinguished for the studied region; their seismic potentials were assessed, their orientations (trends) and probable seismogenic slip kinematics were revealed. Table 4 summarizes these data.

Figure 6 illustrates the map of PES zones of the Magadan region with indicated epicenters of moderate to strong ($M_S \geq 4.3$, Fig. 6a) and weak ($M_S \leq 4.2$, Fig. 6b) earthquakes. We can see that earthquake epicenters, given the errors in determination of their coordinates, predominantly coincide with the distinguished PES zones. This is especially relevant to the strong and moderate earthquakes (Fig. 6a). Such a coincidence is far from ideal, but it would be unrealistic to expect a different pattern, given the degree of tectonic knowledge of the region and the accuracy of epicenter determination.

Let us briefly characterize the PES zones presented in Table 4 (the numerals in text correspond to them in the table).

(1) The Ulakhan zone was distinguished on the basis of the largest seismoactive fault of the same name. The zone trends to the northwest and extends more than 700 kilometers. The different kinematics of recent motions is reported in the zone, with the pre-

Table 3. Fragment of the matrix of seismic activity $A_{3.3}$

φ/λ	143.70	144.00	144.30	144.70	145.00	145.30	145.70	146.00	146.34	146.70	147.00
59.00	0.001	0.001	0.001	0.001	0.001	0.001	0.001	0.001	0.001	0.001	0.001
59.17	0.003	0.003	0.001	0.001	0.001	0.001	0.001	0.001	0.001	0.001	0.001
59.33	0.004	0.005	0.001	0.004	0.007	0.003	0.001	0.001	0.001	0.002	0.005
59.50	0.001	0.004	0.002	0.004	0.007	0.003	0.001	0.001	0.003	0.013	0.028
59.67	0.001	0.005	0.004	0.001	0.003	0.003	0.002	0.011	0.01	0.014	0.025
59.83	0.001	0.003	0.003	0.001	0.004	0.004	0.005	0.017	0.013	0.003	0.003
60.00	0.001	0.001	0.004	0.004	0.006	0.007	0.006	0.01	0.005	0.001	0.006
60.16	0.007	0.01	0.01	0.006	0.004	0.005	0.004	0.003	0.001	0.001	0.004
60.33	0.007	0.009	0.006	0.003	0.001	0.001	0.001	0.001	0.001	0.001	0.001
60.50	0.003	0.004	0.001	0.001	0.001	0.001	0.001	0.003	0.009	0.008	0.006
60.66	0.003	0.004	0.002	0.009	0.015	0.009	0.001	0.003	0.012	0.01	0.007
60.83	0.001	0.001	0.004	0.011	0.017	0.009	0.001	0.001	0.004	0.004	0.003
61.00	0.001	0.008	0.009	0.004	0.006	0.005	0.005	0.006	0.003	0.001	0.001
61.16	0.002	0.008	0.012	0.016	0.014	0.008	0.01	0.012	0.007	0.001	0.001
61.33	0.002	0.005	0.01	0.024	0.025	0.016	0.01	0.009	0.008	0.001	0.001
61.50	0.001	0.009	0.018	0.021	0.023	0.017	0.006	0.006	0.006	0.001	0.002

dominance of left-lateral strike-slips and oblique (with a normal-dip component) strike-slips. This zone hosts several sources of strong earthquakes and a series of weaker ones (UAC, Fig. 6). In addition, tectonic and gravitational paleoseismodislocations have been revealed here. In this respect, the seismic potential of this zone is assessed as very high, with $M_{max} = 7.5$.

(2) The Dapir zone joins the Ulakhan zone at an acute angle. It was named after the large regional fault, 500 kilometers in length. The predominant kinematics in the zone are oblique (reverse-dip) strike-slips. The zone is well traced in satellite images, and swarms of paleoseismodislocations were revealed here (Vazhenin et al., 1997). The seismic potential is assessed at $M_{max} = 7.5$.

(3) The Chai-Yur'ya zone trends to the northwest and can be seen well in satellite images. It was named after the large active fault of the same name and is 750 kilometers long. The zone hosts many earthquakes and their traces; one of the strongest events was the Artyk one with $M = 7.1$ (Kondorskaya and Shebalin,

Table 4. PES zones in the territory of Magadan region

Nos.	PES zone	Trend	Slip type	M_{max}
1	Ulakhan	NW	Sinistral strike-slip and oblique thrust	7.5
2	Dapir	NW	Oblique strike-slip	7.5
3	Chai-Yur'ya	NW	Oblique strike-slip transiting to thrust	7.5
4	Yana	NW	Strike-slip with a thrust component	7.0
5	Arga-Tas	NW	Sinistral strike-slip	7.0
6	Umara	NW	Reverse dip and thrust	6.5
7	Omchak	NW	Listric normal dip	6.5
8	Inya	NE	–	6.5
9	Inya-Yama	E–W	–	6.5
10	Pautovaya	NE	Thrust	6.5
11	Chelomdzha-Yama	E–W	Thrust	7.0
12	Siglan	NE	Strike-slip, oblique strike-slip	7.5
13	Lankovaya-Omolon	NE	Oblique strike-slip	7.0

(a)

(b)
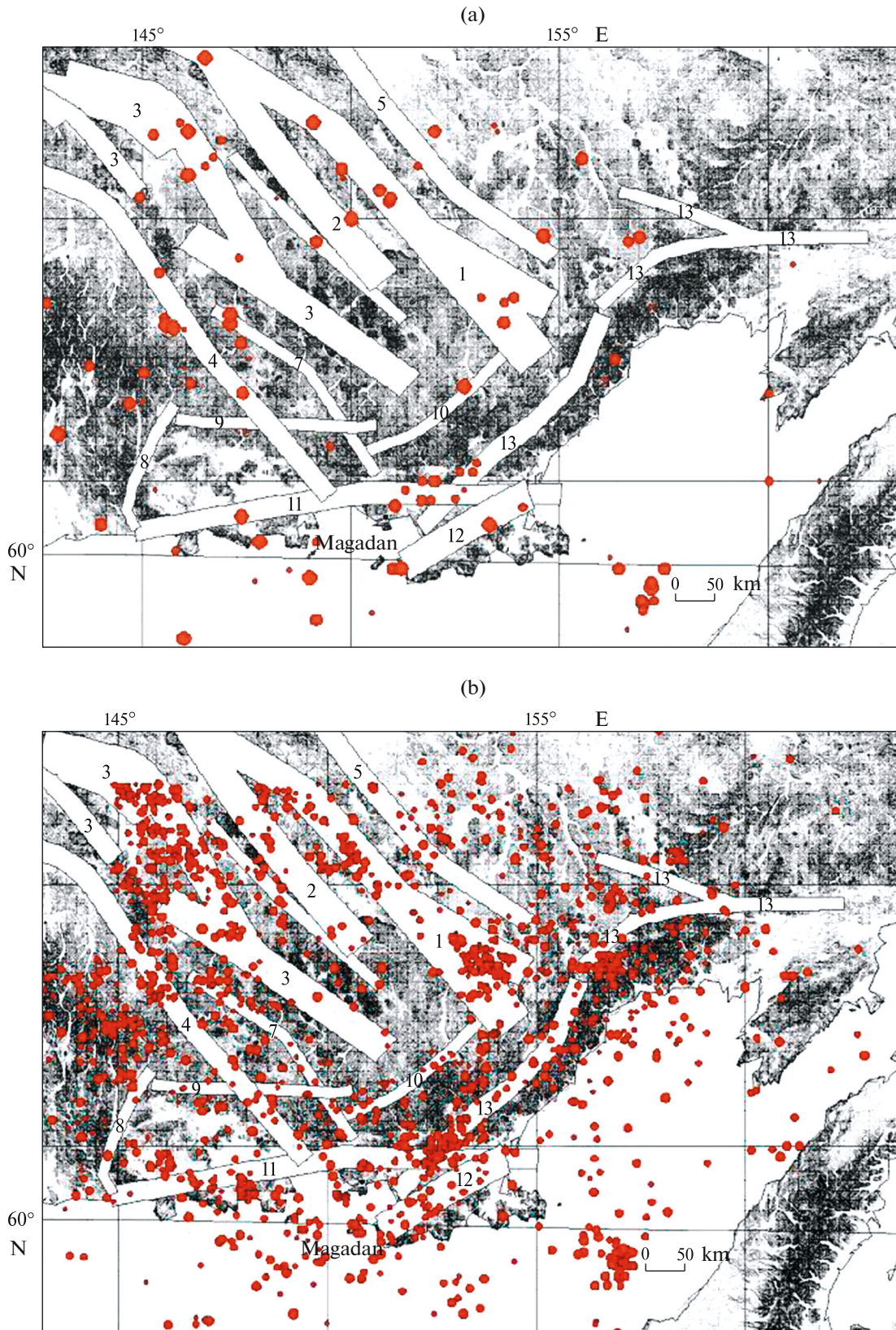
Fig. 6. PES zones of Magadan region. The numbers of PES zones correspond to those in Table 4, where the seismic potentials of the respective zones are given. (a) Epicenters of moderate and strong earthquakes ($4.5 \leq M_S \leq 7.0$); (b) epicenters of weak earthquakes ($2.5 \leq M_S \leq 4.0$). Diameters of circles are proportionate to magnitudes.

1977). Based on these data, the seismic potential of this zone is $M_{max} = 7.5$.

(4) The Yana zone trends to the northwest; it was distinguished on the basis of the fault zone of the same name. Kinematic slip type within this zone is a strike-slip with a thrust component. The zone is well expressed in topography and hosts several strong earthquakes. The seismic potential is assessed at $M_{max} = 7.0$.

(5) The Arga-Tas zone trends to the northwest; it was distinguished along the large fault of the same name. The chain of magnetic field anomalies fits this zone (Imaev et al., 2000). The morphology of this zone suggests sinistral strike-slip kinematics. Its seismic potential is $M_{max} = 7.0$.

(6) The Umara zone was distinguished on the basis of the deep fault of the same name, dividing recent uplifts which sharply differ in amplitude. The difference in amplitude of neotectonic movements is up to 1000 meters, and kinematics of slips are represented by upthrow and thrust. The NW-trending zone is well expressed in topography. Its seismic potential is $M_{max} = 6.5$.

(7) The Omchak zone trends to the northwest. Its kinematic slip type is a listric upthrow. This zone hosts several large earthquakes and a series of weaker ones (Fig. 6). The seismic potential of this zone is assessed at $M_{max} = 6.5$.

(8) The Inya zone trends to the northeast and was distinguished predominantly from satellite images and paleoseismodislocations. The seismic potential is assessed at $M_{max} = 6.5$.

(9) The Inya-Yama zone was distinguished on the basis of the active fault of the same name, consisting of several en echelon fragments, each tens of kilometers long. The zone trends sublatitudinally by a distance of 400 kilometers. Gravitational and tectonic seismodislocations are revealed here. Its seismic potential is assessed at $M_{max} = 6.5$.

(10) The Pautovaya zone trends to the northeast. It was distinguished from paleoseismodislocations and satellite images. The series of rock falls and a large NE-trending fault of up to 40 kilometers long were distinguished within the limits of this zone (Vazhenin et al., 1997). This zone hosts one large earthquake and a series of weaker ones (Fig. 6). Its seismic potential is $M_{max} = 6.5$.

(11) The Chelomdzha-Yama zone is of sublatitudinal trend. It was distinguished on the basis of the large fault of the same name and is about 800 kilometers long. The slip kinematics are of oblique thrust type, with a sinistral strike-slip component. The zone is well expressed in satellite images; additionally, tectonic and gravitational paleoseismodislocations were revealed here (Vazhenin et al., 1997). Its seismic potential is $M_{max} = 7.0$.

(12) The Siglan zone was distinguished on the basis of the large fault of the same name. It trends to the

northeast, is well expressed in topography, and is clearly distinguishable in satellite images. It hosts strong earthquakes and magnitudes of up to $M_S = 7.0$ (UAC) occurred in recent years. In this respect, its seismic potential is assessed at $M_{max} = 7.5$.

(13) The Lankovaya-Omolon zone was distinguished on the basis of the fault zone of the same name. It trends to the northeast and can be generally considered a system of elongated deep oblique (normal-dip) dextral strike-slips, inherited from the Paleogene and causing the formation of different dislocations. This zone also contains swarms of paleoseismodislocations, revealed by B.P. Vazhenin et al. (1997). Its seismic potential is $M_{max} = 7.0$.

The background seismic level assumed for the rest of the area is $M_{max} = 5.0$. The scheme of PES zones (Fig. 6) was digitized with the same step as the matrix $A_{3.3}$, and then converted to the matrix of M_{max}, which, in turn, was used to calculate seismic shaking intensity.

PROBABILISTIC SEISMIC HAZARD ASSESSMENT FOR THE MAGADAN REGION

The probabilistic seismic hazard assessment (PSHA) is based on the calculation of seismic shaking. The initial data for assessing seismic shaking (*Seismicheskaya sotryasaemost'*..., 1979) were the following.

(1) The scheme (matrix) of M_{max}, where cells characterized by some maximal expected magnitude (inferred from seismological and geological-geophysical data) were distinguished. The map of M_{max} for the Magadan region is shown in Fig. 6.

(2) The scheme (matrix) $A_{3.3}$ of seismic activity, which enables us to assess the inherent earthquake recurrence interval, depending on magnitude $M < M_{max}$, for each PES zone.

(3) The slope factor b of the recurrence graph, which determines, along with seismic activity, recurrence intervals for earthquakes of different magnitudes within the distinguished zones. In this case, in accordance with formula (2), we assumed $b = -0.880$.

(4) The macroseismic field equation providing the correlation between the observed macroseismic intensity, earthquake magnitude, epicentral distance, and focal depth. In our calculations we used the macroseismic field equation proposed for the Russian Northeast (*Seismicheskaya sotryasaemost'*..., 1979):

$$I = 1.5M_S - 3.0\log R + 2.5, \qquad (4)$$

where R is the distance between earthquake hypocenter and observation point, i.e., $R = \sqrt{(\Delta^2 + h^2)}$, where, in turn, Δ and h are the epicentral distance and focal depth, respectively, both in kilometers.

(5) The data on average depths of earthquake sources. In our calculations, in accordance with the obtained distributions of hypocenters on depth, we assumed $h = 10$ kilometers.
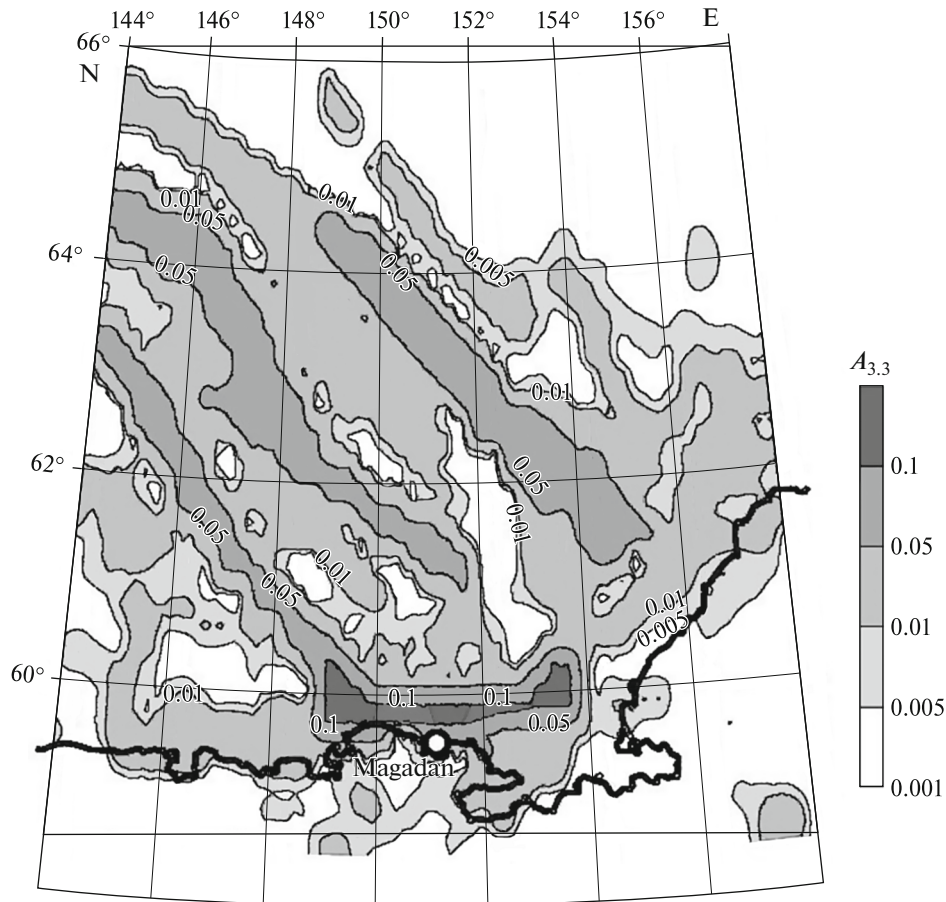
**Fig. 7.** Map of seismic activity $A_{3.3}$ of the Magadan region.

When calculating seismic shaking, we used the map of seismic activity $A_{3.3}$, slightly altered in accordance with the map of PES zones (Fig. 6): the same seismic activity was assumed for each PES zone and numerically it equaled the maximum activity reported in this zone according to $A_{3.3}$. The map of $A_{3.3}$, converted that way, is presented in Fig. 7, where one can see that the converted $A_{3.3}$ map is similar to the map of PES zones to a certain degree.

The calculation of seismic shaking in a particular point (cell of seismic shaking matrix) was performed by numerical integration of seismic effects from all seismic sources (cells of the matrix M_{max}) within the study area at this point, taking into consideration the average recurrence interval for earthquakes with different magnitudes at these points (respective cells of the seismic activity matrix), from the lowest representative one to M_{max} inclusively. Notably, the average recurrence interval for earthquakes with $M \leq M_{max}$ was determined in every cell of the matrix M_{max} based on the value of seismic activity $A_{3.3}$ in the same cell and on the slope factor of the recurrence graph (*Seismicheskaya sotryasaemost'*..., 1979).

The calculation of macroseismic intensity in the Magadan region was performed using special software implemented as a MS Excel macros (facilities of the GS RAS and Schmidt Institute of Physics of the Earth, RAS), whose core was the algorithm for calculating seismic shaking (B_I). The initial data for this software were (1) the matrix of seismic activity $A_{3.3}$ (digital analog of Fig. 7), (2) the matrix M_{max} (digital analog of Fig. 6), (3) slope factor $b = -0.880$, (4) parameters of the macroseismic field equation in the form as in Eq. (4); and the depth of seismoactive layer $h = 10$ kilometers. Also, the average recurrence interval T_{av} is set in years (for example, $T_{av} = 500$, 1000 years, and so on), for which the matrix of shaking intensity (with the same structure as the matrices $A_{3.3}$ and M_{max}) is calculated.

Figure 8 presents the probabilistic maps of seismic hazard for the Magadan region, in macroseismic intensity points, calculated for average recurrence intervals of 500, 1000, and 5000 years.

As was to be expected, the obtained maps of seismic shaking intensity generally repeat the maps of M_{max} and $A_{3.3}$. The highest values of macroseismic intensity are observed in the zones with high seismic
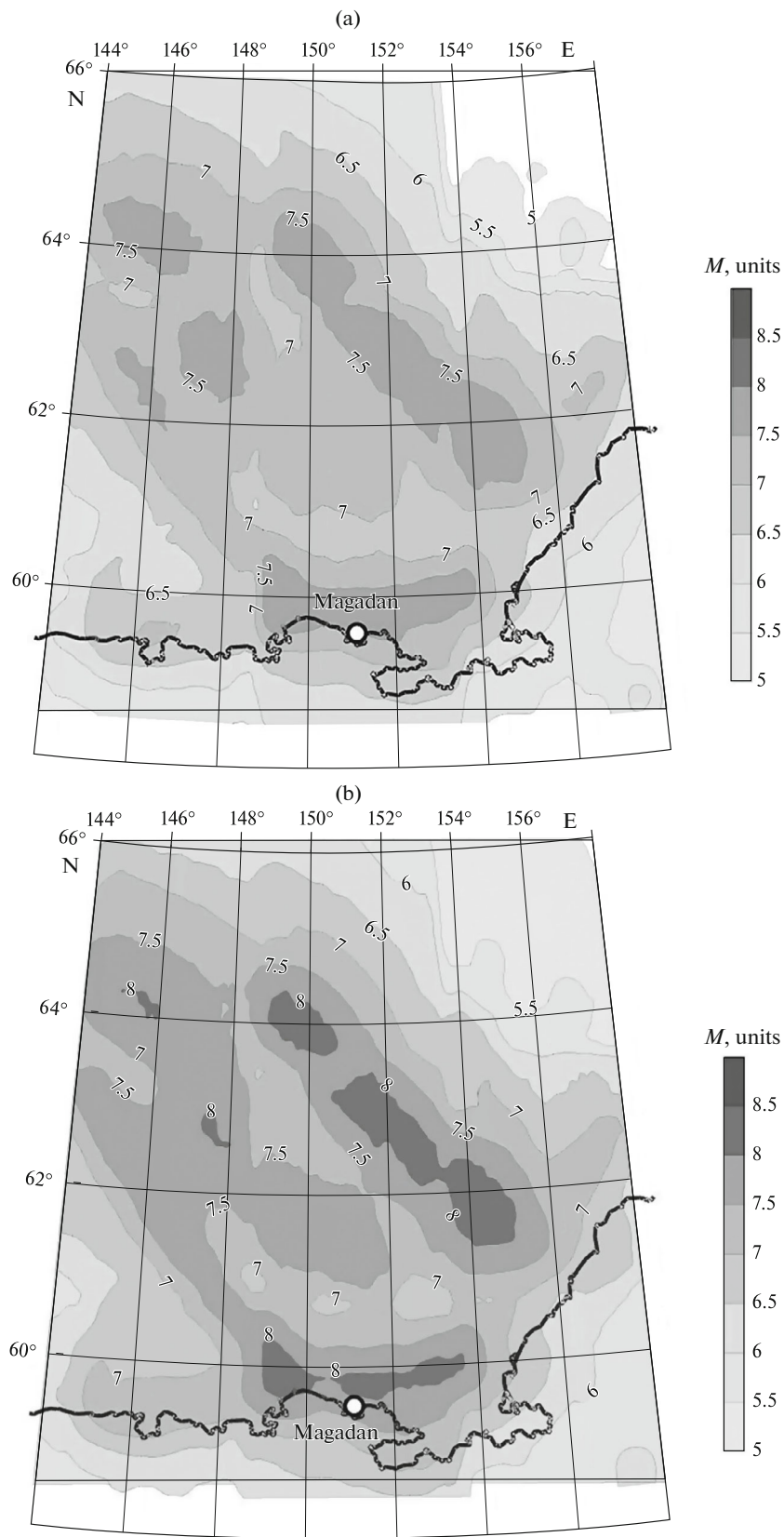
Fig. 8. Maps of macroseismic intensity for the Magadan region at average recurrence intervals of seismic events of (a) 500, (b) 1000, and (c) 5000 years. Numerals denote the intensities of isolines.

(c)
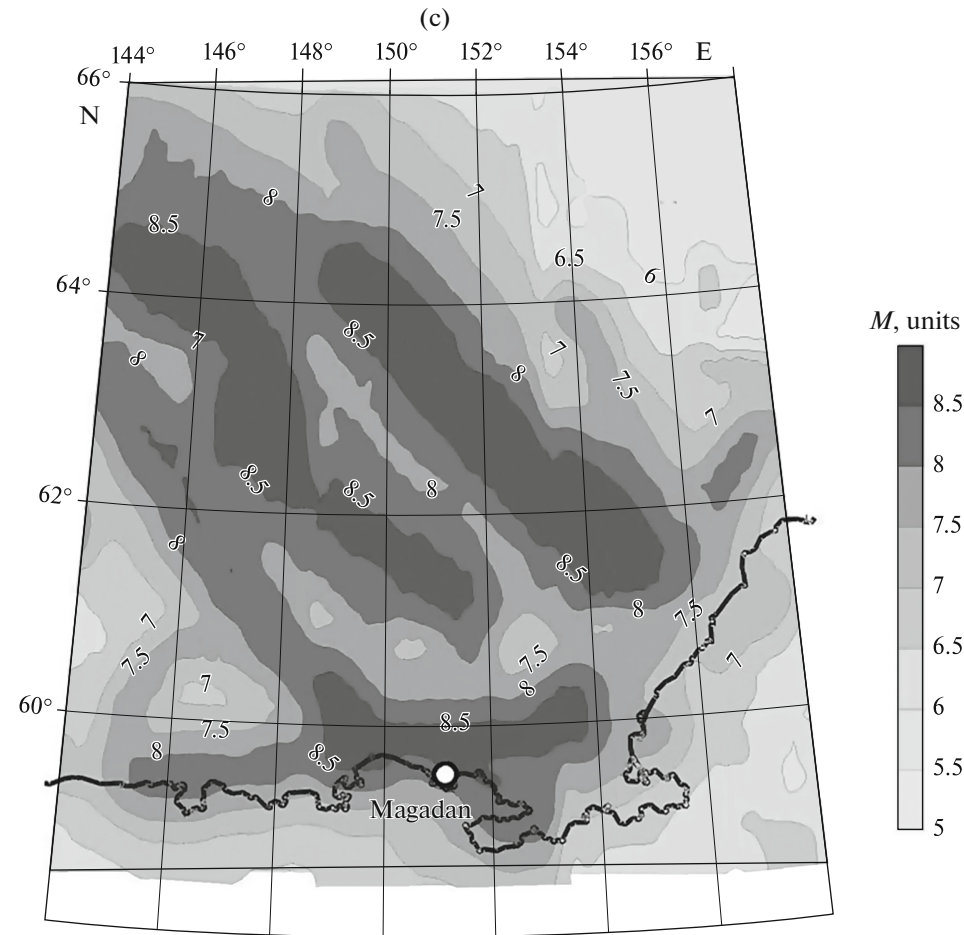
potential ($M_{max} \sim 7.0–7.5$). The maximum shaking intensity changes from $I = 7.5$ at $T_{av} = 500$ years to $I = 8.8$ at $T_{av} = 5000$ years. In general, the calculated shaking intensity appeared to be slightly lower than that in the GSZ-97 and GSZ-2015 maps, and the obtained maps of shaking intensity are more differentiated than those in the GSZ-2015 set.

In Fig. 8 one can see that the city of Magadan is characterized by quite a high level of seismic hazard: it is located at the boundary between two zones with intensities (hereinafter, fractional intensity is provided) 7.0 and 7.5 at $T_{av} = 500$ years, 7.5 and 8.0 at $T_{av} = 1000$ years, and 8.0 and 8.5 at $T_{av} = 5000$ years.

CONCLUSIONS

A seismic hazard assessment for the Magadan region (58.5°–66.0° N, 143.3°–157.7° E) in terms of macroseismic intensity points was carried out using Riznichenko's method (*Seismicheskaya sotryasaemost'...*, 1979), which is based on the calculation of seismic shaking. We estimated the main parameters of seismic regime: slope of the recurrence graph ($b =$

-0.880), matrix of seismic activity $A_{3.3}$, and average thickness of the seismoactive layer and its average depth h (on the basis of these, the value assumed in shaking intensity maps is $h = 10$ kilometers).

Based on the analysis of the complex of seismological, tectonic, and geological data, 13 PES zones with $M_{max} = 6.5, 7.0,$ and 7.5 were distinguished in the territory of the Magadan region. Beyond the distinguished PES zones, background M_{max} was assumed to be 5.0.

An important element of the present work is that when calculating the seismic intensity maps, we used the matrix of seismic activity, corrected in accordance with the map of PES zones: within the limits of each PES zone, the same seismic activity was assumed, namely, the one equal to the maximum observed in the given zone.

As a result of the present work, we have obtained the probabilistic maps of seismic hazard for the Magadan region in terms of macroseismic scale units, for average recurrence intervals of 500, 1000, and 5000 years. These shaking intensity maps generally fit to the maps of M_{max} and seismic activity $A_{3.3}$. The highest val-

ues of macroseismic intensity are observed in the zones with high M_{max} values (M_{max} ~7.0–7.5). The maximum intensity units ranges from $I = 7.5$ at average recurrence interval $T_{av} = 500$ years to $I = 8.8$ at $T_{av} = 5000$ years. In general, the calculated intensity values appeared to be slightly lower than in the GSZ-97 and GSZ-2015 maps.

Owing to a high degree of detail of the seismological and seismotectonics studies conducted in the framework of the present work, the obtained maps have been more differentiated than those in the GSZ-2015 set.

The city of Magadan is characterized by quite a high level of seismic hazard: it is located at the boundary between two zones with intensities 7.0 and 7.5 at $T_{av} = 500$ years, 7.5 and 8.0 at $T_{av} = 1000$ years, and 8.0 and 8.5 at $T_{av} = 5000$ years.

ACKNOWLEDGMENTS

FUNDING

CONFLICT OF INTERESTS

The authors claim no conflict of interest.

REFERENCES

Aleshina, E.I., Kurtkin, S.V., Karpenko, L.I., and Sedov, B.M., Russian Northeast, in *Zemletryaseniya Severnoi Evrazii (2012 g.)* (Earthquakes in Northern Eurasia in 2012), Obninsk: Edinaya Geofiz. Sluzhba Ross. Akad. Nauk, 2018, pp. 197–204.

Bachmanov, D.M., Kozhurin, A.I., and Trifonov, V.G., The database of active faults of Eurasia, *Geodin. Tektonofiz.*, 2017, vol. 8, no. 4, pp. 711–736.
https://doi.org/10.5800/GT-2017-8-4-0314

Bespalov, D.A., Analysis of spatiotemporal regularities of the earthquakes distribution in Magadan region, based on the results obtained in the program for seismic activity calculation, in *Geofizika, geofizicheskie metody poiskov poleznykh iskopaemykh. Materialy konferentsii* (Geophysics, and Geophysical Methods of Search for Mineral Resources: Proceedings of the Conference), 2015, pp. 489–492.
http://vsegei.ru/ru/conf/summary/mnpk-15/theses/09geophis.pdf

Global Centroid Moment Tensor Project, Earthquake Catalog. https://www.globalcmt.org/CMTsearch.html. Accessed November 15, 2019

Gosudarstvennaya geologicheskaya karta. Masshtab 1 : 1000000. Novaya seriya, Leesty O-56 − Magadan; R-56-57 − Ceimchan (s ob"yasnitel'noi zapiskoi) (State Geologic Map, Scale 1 : 1000000. New Series, Sheets O-56 (Magadan) and P-56-57 (Seimchan), with Explanatory Note), Gel'man, M.L., Ed., St. Petersburg: VSEGEI, 1992.

Imaev, V.S., Imaeva, L.P., and Koz'min, B.M., *Seismotektonika Yakutii* (Seismotectonics of Yakutia), Moscow: GEOS, 2000.

Imaev, V.S., Imaeva, L.P., Smekalin, O.P., Koz'min, B.M., Grib, N.N., and Chipizubov, A.V., Seismotectonic map of East Siberia, *Geodin. Tektonofiz.*, 2015, vol. 6, no. 3, pp. 275–287.
https://doi.org/10.5800/GT-2015-6-3-0182

Koz'min, B.M. and Andreev, T.A., Yakutia and Russian Northeast (1735–1974, $M \geq 4.5$, $I_0 \geq 5$), in *Novyi katalog sil'nykh zemletryasenii na territorii SSSR s drevneishikh vremen do 1975 g.* (New Catalog of Strong Earthquakes in the USSR from Ancient Times trough 1975), Kondorskaya, N.V. and Shebalin, N.V., Eds., Moscow: Nauka, 1977, pp. 339–348.

Novyi katalog sil'nykh zemletryasenii na territorii SSSR s drevneishikh vremen do 1975 g. (New Catalog of Earthquake in USSR from Ancient Times trough 1975), Kondorskaya, N.V. and Shebalin, N.V., Eds., Moscow: Nauka, 1977.

Mackey, K., Fujita, K., and Ruff, L., Crustal thickness of northeast Russia, *Tectonophysics*, 1998, vol. 284, pp. 283–297.

Mishin, S.V. and Khasanov, I.M., Seismic activity of Magadan region for the 40-year period, *Geofizika*, 2016, no. 1, pp. 72–74.

Riznichenko, Yu.V., Size of a source of a crustal earthquake and seismic moment, in *Issledovaniya po fizike zemletryasenii* (Studies in Earthquake Physics), Moscow: Nauka, 1976, pp. 9–27.

Seismicheskaya sotryasaemost' territorii SSSR (Seismic Shaking in the Territory of USSR), Riznichenko, Yu.V., Ed., Moscow: Nauka, 1979.

Smirnov, V.N., Northeast Eurasia, in *Noveishaya tektonika, geodinamika i seismichnost' Severnoi Evrazii* (Recent Tectonics, Geodynamics, and Seismicity of Northern Eurasia), Grachev, A.F., Ed., Moscow: PROBEL, 2000, pp. 120–133.

Sharafutdinov, V.M., Development and formation of the 'Seismicity of Magadan region' geoinformation system and its applicability, *Geoinformatika*, 2009, no. 3, pp. 52–56.

Spetsializirovannyi katalog zemletryasenii dlya zadach obshchego seismicheskogo raionirovaniya territorii Rossiiskoi Federatsii (Specialized Earthquake Catalogue for the Purposes of General Seismic Zoning of the Territory of Russian Federation), Ulomov, V.I. and Medvedeva, N.S., Eds., Moscow: Inst. Fiz. Zemli Ross. Akad. Nauk, 2013. http://seismos-u.ifz.ru/documents/Eartquake-Catalog-CK3.pdf

Vazhenin, B.P., *Printsipy, metody i rezul'taty paleoseismogeologicheskikh issledovanii na Severo-Vostoke Rossii* (Principles, Methods, and Results of Paleoseismogeological Studies in the Russian Norteast), Magadan: Severo-Vost. Kompleks. Nauchno-Issled. Inst. Dal'nevost. Otd. Ross. Akad. Nauk, 2000.

Vazhenin, B.P., Mishin, S.V., and Sharafutdinova, L.V., *Zemletryaseniya Magadanskoi region i* (Earthquakes of Magadan Region), Magadan: Severo-Vost. Kompleks. Nauchno-Issled. Inst. Dal'nevost. Otd. Ross. Akad. Nauk, 1997.

Wells, D.L. and Coppersmith, K.J., New empirical relationships among magnitude, rupture length rupture width, rupture area, and surface displacement, *Bull. Seismol. Soc. Am.*, 1994, vol. 84, no. 4, pp. 974–1002.

Translated by N. Astafiev